IOP Publishing Journal of Physics: Condensed Matter
J. Phys.: Condens. Matter **26** (2014) 394008 (12pp) doi:10.1088/0953-8984/26/39/394008

The impact of structural relaxation on spin polarization and magnetization reversal of individual nano structures studied by spin-polarized scanning tunneling microscopy

Dirk Sander[1], Soo-Hyon Phark[1], Marco Corbetta[1], Jeison A Fischer[1,2], Hirofumi Oka[1] and Jürgen Kirschner[1]

[1] Max Planck Institute of Microstructure Physics, Weinberg 2, 06120 Halle, Germany
[2] Laboratório de Filmes Finos e Superfícies, Departamento de Física, Universidade Federal de Santa Catarina, Florianópolis, SC, Brazil

E-mail: sander@mpi-halle.de

Received 4 February 2014, revised 24 March 2014
Accepted for publication 1 April 2014
Published 12 September 2014

Abstract
The application of low temperature spin-polarized scanning tunneling microscopy and spectroscopy in magnetic fields for the quantitative characterization of spin polarization, magnetization reversal and magnetic anisotropy of individual nano structures is reviewed. We find that structural relaxation, spin polarization and magnetic anisotropy vary on the nm scale near the border of a bilayer Co island on Cu(1 1 1). This relaxation is lifted by perimetric decoration with Fe. We discuss the role of spatial variations of the spin-dependent electronic properties within and at the edge of a single nano structure for its magnetic properties.

Keywords: scanning tunneling microscopy, nano magnetism, spin polarization, magnetization reversal

(Some figures may appear in colour only in the online journal)

1. Introduction: nano magnetism and spin-STM

Nano magnetism is a very active field of research, which contributes to the ever advancing developments of magnetic data storage [1–4] and to the emerging field of spintronics [5–9]. In addition to these applications, fundamental questions also raise the interest in both experimental and theoretical studies in nano magnetism. Magnetization reversal of single nano structures is an example where an *ab initio* based understanding on the electronic level has not been achieved yet [10–13]. In this respect, the magnetic characterization of individual nano structures, with sizes in the range of nm, which contain hundreds to thousands of atoms is called for [14]. This is a demanding topic for both experiment and theory, and some novel aspects that point to the contribution of electron confinement and structural relaxation for the spatial variation of spin-dependent electronic properties of individual nano structures are presented here.

Our quantitative studies by spin polarized scanning tunneling microscopy (spin-STM) identify the role of spin-dependent electron confinement for the spatial modulation of the spin-polarization at the surface of a Co nano structure [15]. This finding also has significant impact on spin-dependent transport properties such as the tunnel magneto resistance and its spatial variation on a single nano structure [16]. These results indicate the spatial extent of an inverted spin polarization in nm proximity to the rim of the nano structure as compared to its center. Spatially inhomogeneous properties are also revealed in our quantitative analysis of magnetization reversal of individual Co nano islands [17]. Here, the analysis suggests that only the core of the Co island contributes to the magnetic anisotropy, whereas the Co rim is magnetically soft [17].

This peculiar behavior of the spatial variation of the spin polarization and of the magnetic anisotropy is changed by perimetric decoration of the Co rim. Upon decoration of the

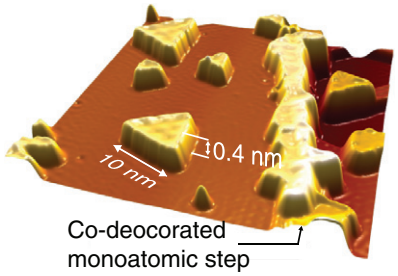

Figure 1. 3D view of a 45 × 34 nm^2 constant current STM image of bilayer Co islands and a Co-decorated step edge on a Cu(1 1 1) surface at 8 K (U_{gap}=+0.1 V, I_t=1 nA). The image illustrates that deposition of Co at 300 K leads to the formation of various nano structures. Individual bilayer Co islands of different sizes, and an extended Co stripe, decorating a monoatomic step of the Cu(1 1 1) substrate, are formed.

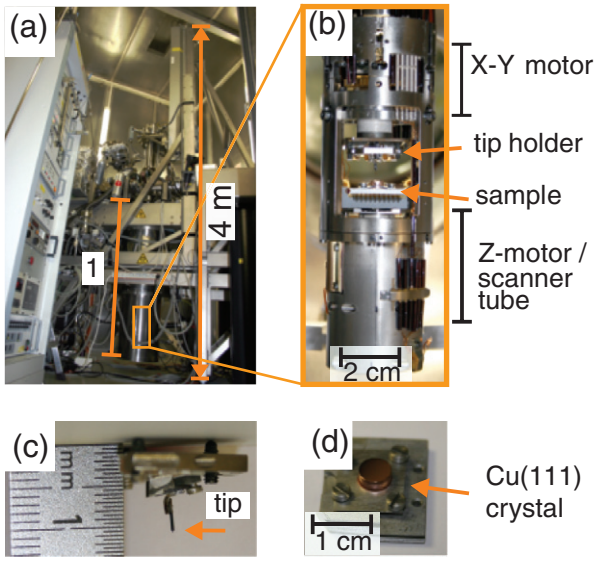

Figure 2. (*a*) The UHV system includes a Janis [49] LHe cryostat (1), which contains a superconducting magnet for fields of up to 7 T along the vertical direction. It also cools the STM by thermal contact with a LHe-cooled plate to 8 K. A long travel manipulator is used to lower the Omicron [50] STM into the cryostat. (*b*) View of the STM head. Both, sample and tip are exchanged *in situ* under UHV at room temperature in the UHV chamber located above the cryostat with the help of Ferrovac [51] wobble sticks. (*c*) Tip holder. (*d*) Sample plate. Note the bores for the handling with the wobble stick. Please consult reference [14] for further details.

bilayer Co island by Fe, we observe a constant sign of spin polarization throughout the Co core, and also all Co atoms contribute to the magnetic anisotropy.

It is the goal of this paper to use spin-STM to shed light onto the physical origin of the impact of perimetric decoration on the magnetic properties of Co nano islands. We discuss the role of structural and electronic relaxation—and the lifting thereof—for the spatial dependence of the spin-dependent electronic properties within an individual Co islands.

Before we discuss this correlation between structural relaxation and spin-dependent electronic properties in greater detail, we want to point out the necessity to characterize individual nano structures. There are a number of magnetic characterization techniques [18], and some give sufficient sensitivity for the magnetic characterization of an assembly of nano structures by collecting integrated data over a larger surface area. Examples are secondary electron microscopy with polarization analysis (SEMPA) [19–21], spin polarized low energy electron microscopy (SPLEEM) [22, 23], magneto-optical Kerr-Effect (MOKE) [24, 25], and x-ray magnetic circular dichroism (XMCD) [26–28]. However, these techniques cannot image and identify single nano structures on the low nm scale. Thus, although the integral magnetic response, such as the area-averaged spin polarization, magnetic susceptibility or dichroic signal is possibly accessible by these techniques, its understanding in view of individual nano structure characteristics is complicated by the distribution of sizes and shapes, which typically characterize an assembly of nano structures. Spatial characterizations within a single nano structure are beyond reach, but they are the realm of STM.

The issue of size and shape distributions of nano structures prepared by self organization is illustrated in the STM image in figure 1. The assembly of nano structures was formed by room temperature deposition of sub-monolayer quantitates Co on Cu(1 1 1). It reveals different morphologies over a 50 nm wide area. Bilayer Co islands of different size, as well as extended Co stripes decorating an atomic step of the Cu substrate are observed. Spin-STM provides the required spatial resolution to not only image these structures, but also to characterize the spin-dependent electronic structure within a single nano structure by spatially-resolved spectroscopy on the atomic scale. Here we present measurements in magnetic fields to extract the dependence of spin polarization and magnetization reversal on island size and perimetric decoration.

The study of the magnetic properties of individual nano structures reveals novel insights into magnetic anisotropy and magnetization reversal, which go far beyond what has been established for thin films and atomic layers [14, 29, 30]. The limited lateral extension of an individual nano structure on the nm scale brings about the decisive impact of lateral structural relaxation and reduced coordination when one strives for the electronic origin of the peculiar magnetic properties on the nanoscale.

The corresponding theoretical description is very demanding. Already for tiny nano structures with some thousand atoms (several nm^3), the self-consistent *ab initio* based structural and magnetic characterization, of e.g. the magnetic anisotropy, is beyond the capabilities of state of the art theory. Thus, it is of utmost importance to provide reliable experimental data on the magnetic properties of individual nano structures for comparison with theory, and the corresponding data are presented here.

This paper is organized as follows. Experimental details are presented next, before we discuss the impact of spin-dependent electron confinement on spin polarization in section 3. Section 4 addresses structural relaxation, its identification by spectroscopy, and the impact of perimetric decoration for lifting structural relaxations near the boundary of a nano structure. Section 5 discusses the quantitative

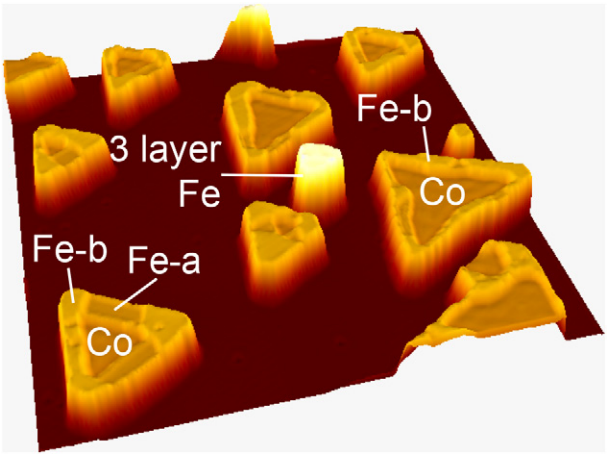

Figure 3. Overview of a constant current STM image obtained after subsequent deposition of sub-monolayer quantitates of first Co, and then Fe on Cu(1 1 1) at 300 K. Bilayer high Co islands are decorated by Fe. Fe grows in two phases, labeled Fe-a and Fe-b, which differ in their stacking. The elemental identification is performed by spectroscopy, as illustrated in figure 4. Note the formation of a three layer tall island, imaged in the center. Image size: 50 × 50 nm^2 (U_{gap} = +0.1 V, I_t = 1 nA).

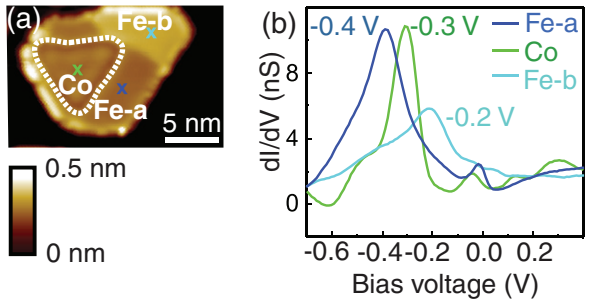

Figure 4. (*a*) Constant current STM image of an Fe-decorated Co island, the Co core is encircled by the dashed white line. (*b*) Differential conductance point spectroscopy measurements at the Co core (green cross), and the Fe-a (dark blue cross) and Fe-b (light-blue cross) area. The areas are identified by their respective peak energies: Co: −0.3 eV, Fe-a: −0.4 eV, Fe-b: −0.2 eV, as outlined in the text. Please refer to figure 9 for spatially resolved spectroscopy of pure and Fe-decorated Co islands.

analysis of magnetization reversal in bilayer Co islands and Fe-decorated Co-islands in view of the magnetic anisotropy of the nano structure.

2. Experimental aspects

STM has become the method of choice to characterize individual nano structures in the size range from individual atoms and molecules up to several ten thousands atoms [31–35]. One peculiarly powerful aspect of STM is that it provides access to the electronic density of states of the tip-sample system by differential conductance spectroscopy with atomic resolution [36–40].

The magnetic sensitivity of spin-STM exploits the dependence of the conductance of the tunnel junction on the relative orientation of tip and sample magnetization [41–45]. This means that tips with a non-vanishing spin-polarization are prepared in spin-STM experiments.

2.1. Low temperature spin-STM in magnetic fields

The results of the spin-STM experiments reflect the spin dependent electronic properties of both tip and sample. Thus, the identification of the magnetic state of the tip is required to draw reliable conclusions about the magnetic state of the sample. The analysis of spin-STM data benefits tremendously from the combination of the STM with a magnetic field. This ensures that the magnetic state of the tip can be irrefutably characterized by exploiting the magnetic field induced changes of the differential conductance of the system [46–48].

As critical temperatures for nano magnetism are often of the order of several K, we combine a LHe cooled STM with a superconducting magnet, which produces a field of seven T. Figure 2 shows the experimental set up used in our laboratory.

An Omicron cryogenic STM [50] is combined with a Janis cryostat [49]. The STM head, shown in figure 2(*b*), is loaded with the tip, figure 2(*c*), and the sample plate, figure 2(*d*), under ultra high vacuum at room temperature. The sample plate can be moved vertically by 10 mm by s stick-slip piezo drive. This facilitates sample exchange without tip damage and it allows one to accommodate different tip lengths. The STM tip can be positioned laterally in both *x* and *y* directions by ±5 mm. The tip is fixed while the sample plate is scanned for the acquisition of a STM image. After sample and tip preparation, the STM is lowered into the cryostat and positioned at the center of a split-coil superconducting magnet, which produces a field of up to 7 T along the vertical direction. The STM cools down from 300 to 8 K within 12 h. At 8 K we obtain a maximum scan range of roughly 800 × 800 nm^2.

2.2. Sample preparation in situ under UHV conditions

The Cu(1 1 1) crystal is cleaned by repeated cycles of ion bombardment and annealing, as described previously [14, 15, 17]. The procedure gives several 100 nm wide atomically clean and flat terraces, which are separated by single layer atomic steps, as checked by STM at 300 K and after cool down at 8 K. Co is deposited onto the clean Cu(1 1 1) surface at 300 K at a rate of approximately 1 atomic layer in 2 min. The deposition of sub-monolayer quantities leads to the formation of predominant bilayer high Co islands and decoration of step edges [52], as shown in figure 1. Subsequent sub-monolayer deposition of Fe under the same conditions leads to a perimetric decoration of the Co bilayer islands, and also to the formation of individual bilayer and trilayer Fe islands. The resulting surface coverage is shown in figure 3. Spatially resolved tunneling spectroscopy of the differential conductance identifies Co and two Fe modifications, as illustrated for an Fe-decorated Co island in figure 4.

The identification of the different areas of the Fe-decorated islands by spectroscopy exploits the previous work on bilayer Co islands on Cu(1 1 1) and on Fe on Cu(1 1 1). We ascribe the spectroscopy peak near −0.3 V to a Co minority state

[15, 53, 54]. Fe forms two phases on Cu(1 1 1). They are discriminated due to their different stacking with respect to the Cu substrate. Fe-a refers to Fe in fcc stacking, whereas Fe-b refers to topmost Fe-atoms in bridge positions. These phases have also been coined 'fcc- and bcc-(*like*) Fe', respectively [55, 56]. The spectroscopic identification of these Fe phases has been established with reference to the atomic structure of Fe on Cu(1 1 1) [55]. Maxima of the differential conductance near −0.2 and −0.4 V identify Fe-b and Fe-a, respectively.

2.3. Tips used in spin-STM

To obtain spin-contrast in STM, we use tips with a spin-polarized apex. Recipes for preparing suitable tips are given in the literature [43, 44, 46, 47, 57, 58]. We use electrochemically etched W-tips, which are briefly heated to 2200 K under UHV conditions, as checked by an optical pyrometer. They are covered by either Fe, Co, Cr or combinations thereof. A film thickness of order 40–100 layers is deposited onto the tip, and annealed at roughly 600 K. Alternatively, bulk Cr tips are also used, and they are introduced into the STM as electrochemically etched from a Cr rod *ex situ* [47].

The tips used in the spin-STM are investigated by field ion microscopy to check the atomic structure at the apex and to independently establish the film thickness from field evaporation [59]. The spin polarization of field emitted electrons from the tips has been studied by spin polarization analysis with a Mott-detector [60]. These characterizations confirm and quantify the spin-polarization of electrons emerging from the tip apex, in agreement with the corresponding analysis of the spin polarization presented in section 3.

For all tips, we scrutinize the presence of a spin-polarized tip apex *in situ* by measuring the differential conductance on Co islands while changing the external magnetic field along the sample normal. Previous spin-STM work has revealed the easy magnetization direction out-of-plane of these Co nano islands [61]. We exploit the variation of the differential conductance as a function of field to obtain a magnetic hysteresis curve of a single nano structure. This procedure is described in the following.

2.4. The extraction of switching fields and spin polarization from spin-STM data

One key feature of the magnetic characterization is the clear identification of states of so-called parallel (P) and anti-parallel (AP) magnetization orientation of tip and sample. The magnetic field induced transition between these states gives the largest magnetic contrast in the differential conductance [41, 62, 63]. The comparison of the spectroscopy signal of both states is the basis to extract the spin polarization of the system.

The tunnel current and also the differential conductance depend on the relative orientation between the magnetization of tip and sample [41, 42, 62], and this dependence gives the spin-dependent contrast in STM. The underlying physical principle is known as tunnel magnetoresistance (TMR), and it is also the basis for the functionality of *e.g.* modern sensors [3, 64, 65]. The external magnetic field is controlled to change

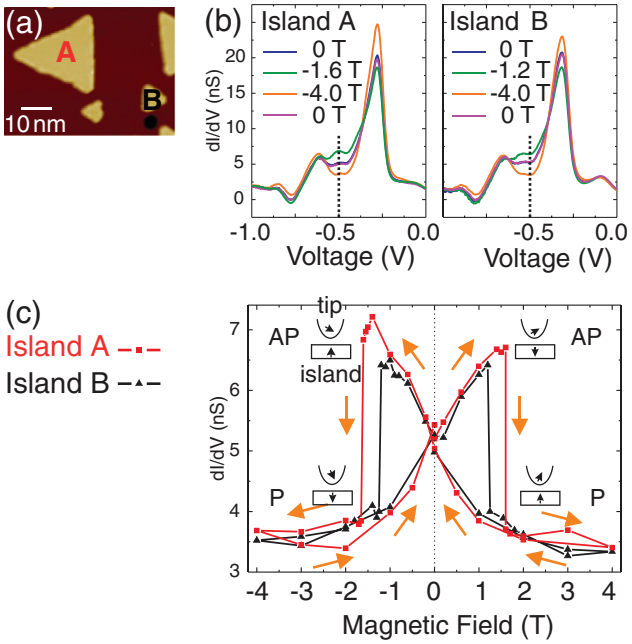

Figure 5. Comparison between topography and spatially resolved spectroscopy between pure Co (top row) and Fe-decorated bilayer Co islands (bottom row). Constant current STM images of a pure Co bilayer island in (*a*) and of a Fe-decorated Co island in (*c*) ($U_{gap} = +0.1$ V, $I_t = 1$ nA). The images show an arrow, along which position dependent spectroscopy data of the differential conductance were taken. The spectra are shown for the pure Co and the Fe-decorated Co island in (*b*) and (*d*), respectively. They are shifted vertically for clarity. Whereas the data for pure Co show a sizable shift of the peak at −0.3 eV to more negative values upon transition towards the edge of the island, the corresponding peak position measured on the Fe-decorated Co island does not show any appreciable shift up to the border with Fe. See text for the discussion.

the relative magnetization orientation between tip and sample [46], inducing a corresponding change of the tunnel current and the differential conductance. The change of the latter in response to the field is shown in figure 5 for measurements on the center of a larger and smaller bilayer Co island at 8 K.

The main feature of the spectroscopy signal is a peak around −0.3 eV, which is ascribed to a Co minority state [53]. With a change of field we see that the peak intensity and also the shape of the spectroscopy curve change. We plot the signal change at −0.5 V in figure 5(*b*) and obtain hysteresis curves [66] of the differential conductance for both islands, as shown in figure 5(*c*). Note, that the inner part of the hysteresis curves around zero T is similar for both islands, whereas the sharp signal change is observed at a larger field of 1.6 T for the larger island, as compared to 1.2 T found for the smaller island. The smooth signal variation for small fields around 0 T is ascribed to the response of the tip to the magnetic field.

The response of the magnetic state of the tip to the field can also be different. We also observe bi-stable tips and tips of constant magnetization orientation [46]. Our empirical observations tell us that the tip behavior is not conclusively determined by the macroscopic tip preparation. Rather, the tip response to the field is largely determined by microscopic changes at the tip apex [46, 48].

Our example of figure 5 indicates that both components, tip and sample respond to the magnetic field. At small fields the tip magnetization follows the direction of the magnetic field, and at a critical value, the so-called switching field, the island magnetization direction reverts from anti-parallel to parallel to the magnetic field, causing a sharp signal change. We extract switching fields of Co and Fe-decorated Co islands for different island sizes, and the quantitive analysis reveals the magnetic anisotropy of the islands, as discussed in section 5.

The discussion of the TMR effect [41, 62] reveals that the spin polarization of both tip and sample determines the magnetic contrast. With respect to figure 5(*c*) this means that the observation of a difference in the differential conductance between a parallel and an anti-parallel spin alignment of tip and sample indicates a non-zero spin polarizations of both tip P_{tip} and sample P_{sample}.

The asymmetry of the differential conductance A is related to the spin polarization of the system. We have $A_{\mathrm{d}I/\mathrm{d}V} = (\mathrm{d}I/\mathrm{d}V_{\mathrm{AP}} - \mathrm{d}I/\mathrm{d}V_{\mathrm{P}})/(\mathrm{d}I/\mathrm{d}V_{\mathrm{AP}} + \mathrm{d}I/\mathrm{d}V_{\mathrm{P}}) = -P_{\mathrm{tip}}P_{\mathrm{sample}}$ [15, 44]. Based on this relation we obtain the spin polarization of the system from measurements which were performed for parallel (P) and anti-parallel (AP) magnetization states. Maps of the asymmetry, calculated from the corresponding differential conductance, are analyzed in the next section to characterize the spatial dependence of the spin-polarization. The asymmetry signal shows a pronounced energy dependence [47, 67, 68]. We compared the energy dependence of the experimental asymmetry with that of the calculated spin-polarization (see supplementary online material of reference [15]). This analysis confirms that the asymmetry signal is indeed related to the spin-polarization of the sample, provided that the the spin-polarization of the tip is taken into account.

3. Spin-dependent electron confinement

The comparable magnitudes of the Fermi wave length, i.e. the wavelength of an electron at the Fermi energy, and the lateral dimensions of nano structures cause interference effects, which drive a pronounced spatial modulation of the electronic density of states within a nano structure [38, 69]. Experimentally, these modulation are observed in maps of the differential conductance [32, 53, 70, 71].

Electron confinement is a spin-dependent phenomenon [72]. Theory has revealed that pronounced spatial oscillations of the spin-resolved local density of states are to be expected [73]. Figure 6 provides examples for maps of the differential conductance measured close to the Fermi energy at +0.03 eV for states of antiparallel (AP) and parallel (P) alignment of tip and sample magnetization.

The maps reveal a pronounced spatial oscillation of the differential conductance, where the spacing between rows of minima is of order 2.5 nm for both maps. We can immediately conclude that the Fermi wavelength is of order 5 nm, as interference extrema in a standing wave pattern are spaced at half wavelength. A more stringent analysis of the dispersion relation is possible by analyzing the modulation patterns as a function of energy, and it confirms this estimate. We find that the modulation patterns are observed only for an energy

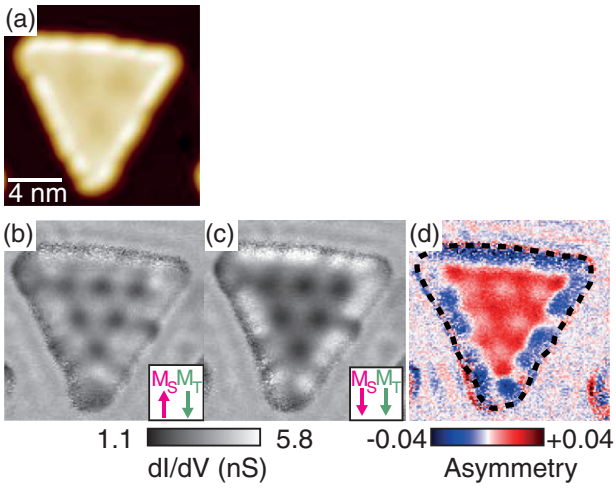

Figure 6. Magnetic characterization of bilayer Co islands in magnetic fields along the sample normal at 8 K. The differential conductance measured at the center of a large (*a*) and a small island (*b*), imaged in (*a*), changes in response to the field, as indicated in (*b*). The signal change at −0.5 V as a function of field is plotted in (*c*), and it reflects a magnetic hysteresis curve of a single nano island. The larger island shows the larger switching field. The small sketches indicate anti-parallel (AP) and parallel (P) states of sample and tip magnetization. The arrows indicate the sequence of field change.

above −0.18 eV, and we observe that the modulation wavelength gets shorter with increasing energy. The corresponding energy dispersion relation can be approximated by a parabolic dispersion up to an energy of +0.3 eV, where the dispersion gets significantly flatter [74, 75].

We stress two important observations [15]. Firstly, the modulation maps of AP and P states vary in their contrast. The contrast is more pronounced for the AP state. Secondly, the modulation pattern does not extend to the edge of the island, but it appears to be limited to the inner core, with no periodic modulation in the outermost rim of approximately 1–2 nm width.

We apply the theoretically derived relation between the asymmetry of the differential conductance and the spin polarization introduced above in section 2.4 to perform image math to obtain a map of the differential conductance asymmetry. The result is shown figure 6(*d*). We see that the asymmetry is modulated around positive values in the core region of the Co island, and it shows a negative value in the rim area. In a previous publication we have shown that we can ascribe the map of the asymmetry to a map of the spin polarization above the Co island. We are led to this conclusion by the favorable agreement between the experimental asymmetry maps and calculated maps of the spin polarization at a height of 0.5 nm above the surface, which reflects the tip-sample distance in the experiment [15].

One example of the favorable correspondence between calculated spin polarization and experimental asymmetry is presented in figure 7. Our calculations are based on density functional theory implemented in the multiple-scattering Korringa–Kohn–Rostoker Greens function method [15]. Thus, we calculate spatially resolved maps of the LDOS

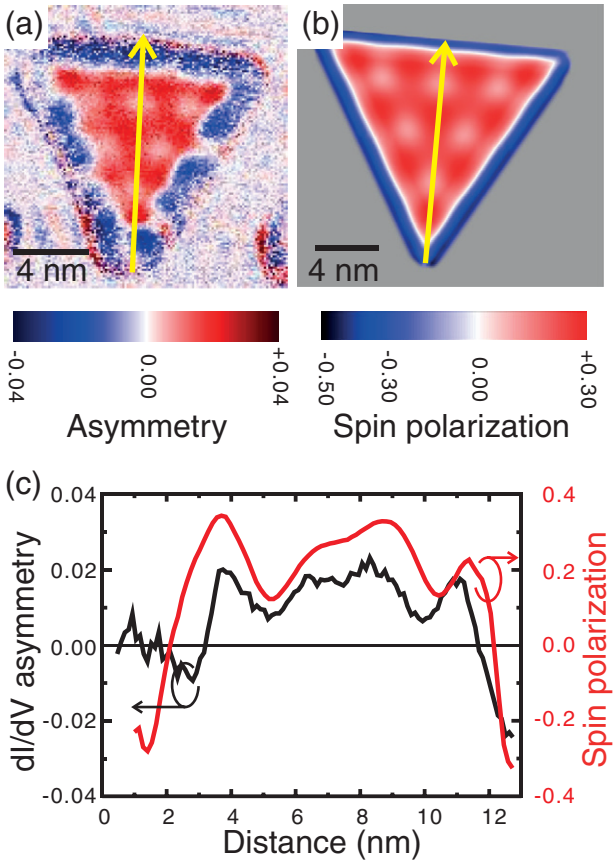

Figure 7. Maps of the differential conductance measured in a field of −1.1 T at 8 K near the Fermi energy (U_{gap} = +0.03 eV) for anti-parallel (AP) (*b*) and parallel (P) (*c*) states, for the bilayer Co island imaged in (*a*). Spatial modulation are observed in the inner part of the island. Calculated asymmetry of the differential conductance in (*d*) from maps (*b*) and (*c*) by image math: asymmetry= (map(*b*)-map(*c*))/(map(*b*)+map(*c*)). Note the inverted asymmetry signal close to the Co rim *within* the Co island. This differs sharply from the asymmetry signal of the Fe-decorated Co island shown below in figure 8, which lacks the inverted asymmetry towards the Co rim. The dashed line in (*d*) shows the topographic border of the Co island of (*a*) as given by the line of half apparent height.

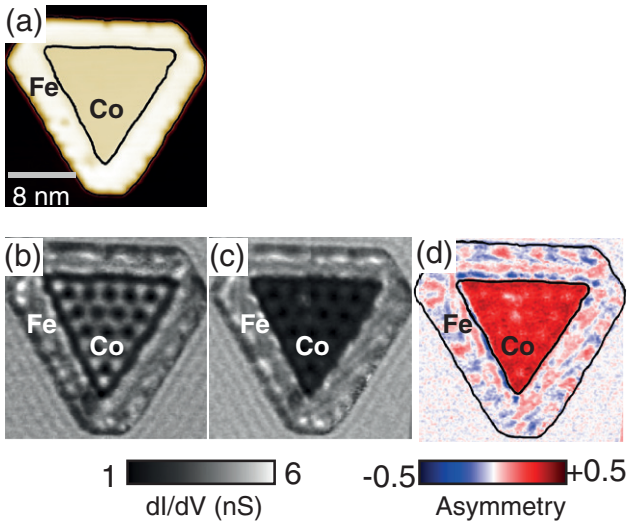

Figure 8. Maps of the differential conductance measured in a field of −1.1 T at 8 K near the Fermi energy (U_{gap} = +0.03 eV) for anti-parallel (AP) (*b*) and parallel (P) (*c*) states, for the Fe-decorated bilayer Co island imaged in (*a*). Spatial modulation are observed in the inner part of the island. Calculated asymmetry of the differential conductance in (*d*) from maps (*b*) and (*c*) by image math, asymmetry= (map(*b*)-map(*c*))/(map(*b*)+map(*c*)). The modulation pattern in (*b*) and (*c*), and the asymmetry in (*d*) extend right towards the rim of the Co core. This differs sharply from the results of figure 6, where already in nm proximity to the Co edge the spectroscopy signals change dramatically.

above a triangular two-atomic-layer Co island on Cu(1 1 1) for majority and minority states, and from this we derive the calculated asymmetry map shown in figure 7.

We compare the experimental asymmetry data along a line scan to the calculated spin polarization along a corresponding line scan of the model system. We see that both experiment and theory find a pronounced spatial modulation in positive values of the signals in the inner part of the Co island. This is ascribed to the larger majority density of states at the Fermi energy, as compared to that of the minority states. This gives a positive spin polarization. As the experimental asymmetry signal is given by $-P_{tip}P_{sample}$, we conclude that a favorable agreement between experiment and theory is given for a spin polarization of the tip of −0.1.

This result and also the successful description of the energy dependence of the asymmetry signal in view of the variation of the spin polarization with energy as discussed in [14, 15] indicate that the asymmetry of the differential conductance can be quantitively related to the spin polarization of the sample. Thus, the spatial variation of the spin polarization on the nm scale is accessible and can be mapped with unsurpassed spatial resolution by spin-STM.

The pronounced spatial modulation of the asymmetry maps reveals that electron confinement is a spin-dependent phenomenon [15, 72]. Majority and minority electrons of the Co are affected differently by electron confinement. Our data indicate that electron confinement acts mainly on the majority electrons. This is a plausible result, as majority electrons in the Co bilayer are of sp-character, whereas the minority electrons are of d-character. The more pronounced spatial localization of d-electrons renders them less susceptible to confinement effects as compared to sp-electrons.

The different sign of the asymmetry at the rim of the island, as shown in figures 6(*d*) and 7(*a*), points at a spatial variation of the electronic structure from the island center towards the island edge [71]. Experimentally, we characterize this variation of the electronic structure by position dependent differential conductance measurements. The spectroscopy data shown in figure 9 below and discussed in section 4 corroborate the impact of structural relaxation on the electronic structure. The data are in line with the assumption of larger Co-Co bond length at the island center as compared to the island edge.

In an effort to modify the peculiar spin-dependent electronic properties near the edge of the Co bilayer island, we decorate its perimeter by room temperature deposition of submonolayer amounts of Fe. Fe forms a bilayer high decoration, surrounding the Co core. An assembly of Fe-decorated Co islands is shown in the constant current image of figure 3 above.

Fe and Co are clearly identified by their respective spectroscopic signatures [53, 55], as shown in figure 4, which also indicate an atomically sharp transition from Co to Fe in figure 9.

This perimetric decoration of the Co core changes the spin-dependent electronic properties near the Co rim, and we demonstrate this in the maps of the differential conductance and the asymmetry, which are presented in figure 8.

In sharp contrast to the images presented above in figure 6 we find that the modulation of the differential conductance in figures 8(*b*) and (*c*) now extends all over the Co area. Upon decoration, the Co boundary does not show up as a region of lacking modulation of the differential conductance. Also, the asymmetry in figure 8(*d*) reveals an electron-confinement induced modulation, which extends all the way to the edge of the Co region. We do not observe a rim area of inverted asymmetry, as shown above in figure 6(*d*) for the pure Co island.

This example shows that we can tune the spatial variation of the spin-dependent electronic properties of an individual nano structure by decoration. This has significant implications for spin-dependent transport, where we expect a much more spatially homogenous behavior of the TMR as compared to that measure on a pure Co island [65].

We ascribe the impact of Fe decoration on the modified spatially resolved spectroscopy to the change of structural relaxation upon Fe decoration. This view is corroborated by our observation in figure 9 of spatially constant energy positions of the minority related 3d-electronic state of Co. Peak shifts and electronic rim states are not observed upon Fe decoration, and this indicates spatially constant bond lengths within the Co core.

In order to arrive at an electronic picture of the underlying physics, we compare the spatial dependence of the differential conductance of a pure and a Fe-decorated Co island in figure 9 [76]. In the following Section we provide a flavor for the main issue.

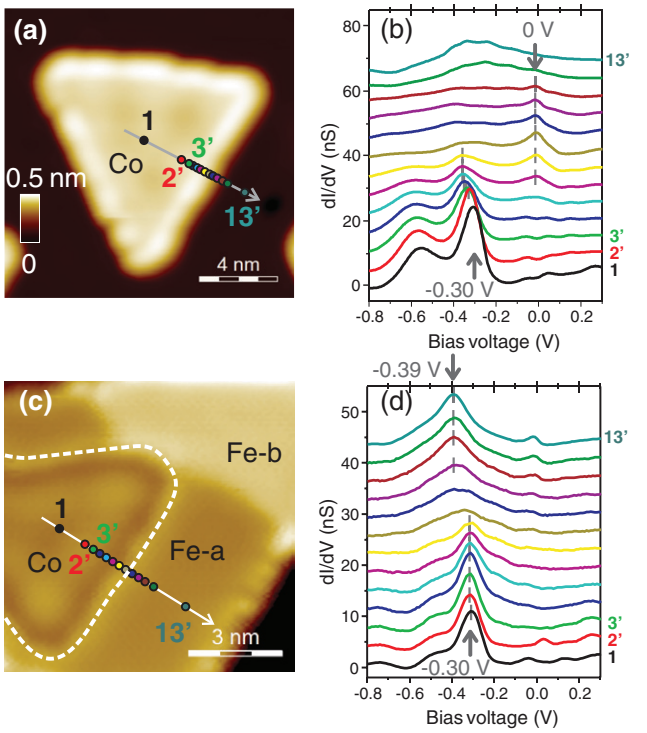

Figure 9. Comparison of a line scan through the asymmetry map of figure 6(*d*) in (*a*) and the calculated spin polarization in (*b*). Plot (*c*) reveals that a favorable agreement between the experimental curve (black, left scale) and the calculated spin polarization (red, right scale) can be achieved for a tip spin polarization of −0.1, as explained in the text.

4. Structural relaxation and position dependent electronic structure

In contrast to epitaxial atomic layers, where lattice misfit, epitaxial strain, vertical layer relaxation are well defined properties [29, 77, 78], for individual nano structures spatial variations of the atomic structures are expected [79, 80] and experimentally observed [81–83]. Here, structural and electronic relaxations on the nanoscale are driven by uncompensated forces and reduced coordination at the boundary of a nano structure. As a result, both atomic positions *and* electronic structure show a pronounced spatial dependence [54, 84, 85]. Thus, any appropriate description of spin-dependent properties stringently requires the consideration of these effects. Note, that concepts such as strain and layer relaxation need to be applied with considerable care, as the atomic distances vary throughout a single nano structure, and the description by a oversimplified strain concept appears questionable. Rather, the description in view of mesoscopic misfit [80, 86] appears to be better suited to address the peculiar bonding situation in nano structures.

The previous and the following Section provide experimental evidence that spin-polarization and magnetic anisotropy in the rim region of individual Co bilayer islands are drastically changed upon perimetric decoration. The spin-polarization becomes spatially more homogeneous, and the magnetic anisotropy of the Co core is reduced upon Fe decoration.

Here we exploit the spatial resolution of the STM to investigate the position dependence of the differential conductance signal [54] within pure and Fe-decorated Co islands. These data provide compelling evidence that structural relaxations in the Co core are lifted upon decoration.

The data of figure 9(*b*) reveal that the energy position of the peak of the differential conductance, which is related to the Co minority states, located near −0.3 eV at the island center, shifts to more negative values towards −0.4 eV close to the island edge [54]. Near the island edge, a novel electronic feature appears in spectroscopy as a peak at the Fermi energy, which has been coined *rim state* [71]. Where it is observed, the intensity of the peak near −0.4 is strongly suppressed.

We ascribe this spatial dependence of the spin-dependent electronic structure in an individual nano island to the impact of both, lattice relaxation and reduced coordination. Previous combined experimental and theoretical studies have identified the intimate link between structural relaxation and electronic structure for this [54] and a related system [85], and we focus on the structural relaxation first.

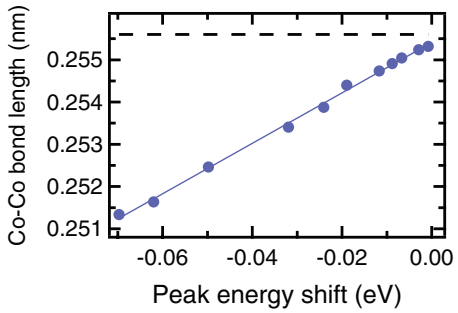

Figure 10. Relation between the average Co–Co bond length of a bilayer Co structure on Cu(1 1 1) and the shift of peak energy of the 3d minority state of Co. The data are extracted from a previous study [54]. The dashed line indicates the Co bond length of 2.556 Å, representing pseudomorphic growth. The blue line is a guide for the eye. The peak energy shifts to more negative values with decreasing bond length.

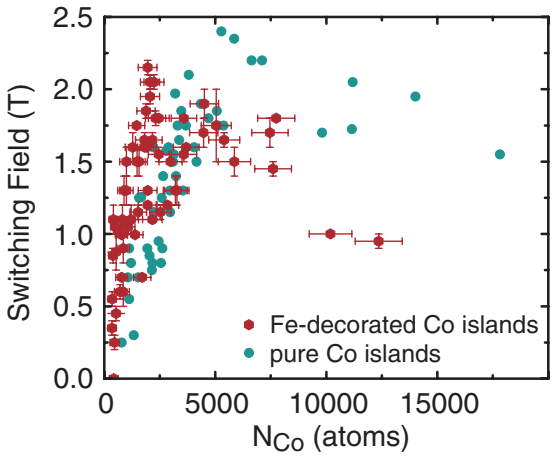

Figure 11. Compilation of switching fields of Co (cyan) and Fe-decorated Co (red) bilayer islands on Cu(1 1 1), measured at 8 K.

The observed shift of the peak energy to more negative values towards the island edge for the island shown in figure 9(*a*) with a base length of 12 nm can be ascribed to a corresponding reduction of the in-plane Co–Co atomic distance. We present the relation between the average Co–Co bond length of Co islands of different size and the peak energy shift in figure 10, as extracted from the published data [54]. The plot shows as a dashed line the Co–Co bond length of 2.556 Å, which serves as a reference indicating the bond length in pseudomorphic positions on Cu(1 1 1). At this bond length a peak energy of −0.3 eV is observed. The plot reveals that a shift of peak energy to more negative values indicates a shorter Co–Co bond length.

The calculations indicate that the Co–Co bond length at the center of a 15 nm size island approaches the value indicative of pseudomorphic growth on Cu(1 1 1). This gives a nearest neighbor distance of $\frac{1}{\sqrt{2}}a_{Cu} = 2.556$ Å, with $a_{Cu} = 3.615$ Å. However, near the island edge a reduced bond length of ≈2.51 Å is found in the calculations. This reduced bond length leads to a peak energy shift of −0.07 eV. The structural relaxation reflects the tendency of epitaxial misfit stress to reduce the Co–Co bond length. This stress is driven by the tensile misfit of $\eta = (a_{Cu} - a_{fccCo})/a_{fccCo} = +1.89$ %, with $a_{fccCo} = 3.548$ Å[87]. As a result, atomic positions change throughout the nano structure, as stresses acting at the boundary of the structure differ from those acting at the island center, and this drives a spatially varying structural relaxation, which affects both topmost and the interface layer in contact with Cu. Note that topmost and interface Co atoms may respond differently to the stress, and the notion of a strain to characterize the bond length on individual nm small islands may be too simplistic. Thus, a complex atomic relaxation is expected, and it is linked to the spatial dependence of the electronic structure, as observed here.

A further contribution which modifies structural and electronic properties is the reduced coordination. The lack of bonding partners inevitably affects all atoms at the boundary of any structure. Whereas an atom within a fcc material is surrounded by twelve nearest neighbors, this coordination shrinks to nine for atoms at the (1 1 1) surface, and to seven for an atom at the ridge of an (1 1 1) island. This reduced coordination leads to an electron redistribution. This influences the atomic spacings, which often get shorter, and it gives rise to surface stress, which is generally tensile [88, 89]. Thus, the position dependence of the electronic properties, and consequently of the atomic structure, is a general phenomenon for nano structures, and it is not limited to epitaxially strained systems [86].

The decisive difference of the position dependent spectroscopy data in figure 9(*d*) as compared to the data shown in (*b*) is an almost constant energy position of the spectroscopy signal from the Co core towards the border upon Fe decoration. This contrasts with the substantial shift in peak energy for the corresponding transition from the center towards the edge of the pure Co island. Also, the electronic signature of the rim state as a peak at the Fermi energy is only observed for the pure Co island, but not for the Fe decorated island.

These observations support the conclusion that structural and electronic relaxation of a pure Co islands are substantially suppressed in the Co core of the decorated island. We demonstrate in the following section, that also the magnetization reversal and magnetic anisotropy of the Co islands are heavily affected by the decoration, leading to a reduced magnetic anisotropy of the Co core upon decoration.

5. Magnetization reversal of bilayer islands

We have analyzed the magnetization reversal of bilayer Co islands of different sizes by extracting the switching field H_{sw} from the sharp signal drop of the magnetic hysteresis curves measured on individual Co islands [14, 17]. This approach is discussed above in section 2.4 and indicated in figure 5(*c*).

We find that the switching field of bilayer islands changes in a non-monotonic manner with island size. For pure Co bilayer islands (Fe-decorated Co islands) containing up to some 7500 (4000) atoms we find that the switching field increases with island size, whereas it decreases for larger islands. This behavior is observed for both pure and Fe-decorated bilayer

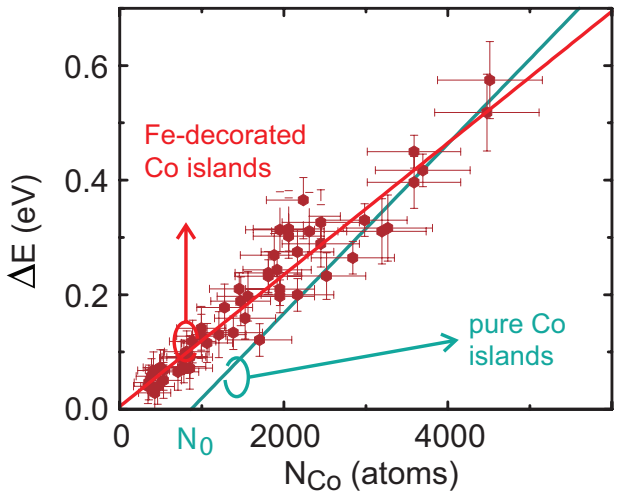

Figure 12. Energy barrier ΔE of magnetization reversal in dependence of island size given by the total number of Co atoms N_{Co}. The data for pure Co islands are described by a linear fit, and only this line (cyan) is shown for clarity. The complete description is given in [17]. The linear fit shows an offset N_0 at the intersection with the horizontal axis. The data of Fe-decorated Co islands (red) extrapolate through the origin of the plot, and they are well described by a linear relation. The slopes of the linear fits give the magnetic anisotropy of the systems.

Co islands, as shown in figure 11. This size dependence of the switching field reflects a general trend due to thermally assisted magnetization reversal [90–93], and its physical origin can be rationalized as follows.

In smaller islands the total magnetic anisotropy is small, and the thermal energy determines the temporal evolution of a magnetic state. As a consequence, very small islands show a superparamagnetic response with vanishing switching fields. With increasing island size the magnetic state acquires temporal stability, and the switching field increases. It approaches the value $2K/M_s$(K: magnetic anisotropy, M_s: saturation magnetization), as given as the maximum possible switching field due to magnetization rotation of a single domain particle in the Stoner–Wohlfarth picture [94]. In larger islands, other reversal processes are conceivable, and the switching field decreases with increasing particle size [2].

Although the switching field data of figure 11 show considerable scatter, we observe that the switching fields tends to increase upon Fe decoration as compared to the pure Co case for a Co island size of up to 4000 atoms. At first sight one might be tempted to conclude that an increased switching field implies a larger magnetic anisotropy. However, this conclusion would be wrong, as only the extraction of the energy barrier of reversal allows a reliable conclusion about the magnetic anisotropy [17].

This analysis in the framework of the Néel-Brown description of thermally assisted reversal gives the energy barrier of magnetization reversal ΔE in dependence of island size [17], and the result is shown in figure 12. This analysis reveals the energy barrier can be described by linear relation with respect to the island size. The slope of the curve gives the magnetic anisotropy.

For pure Co islands the data are represented by the solid line in cyan. Its slope gives a magnetic anisotropy of 0.148 ± 0.005 meV/atom. Surprisingly, this line shows an offset, and it intersects the x-axis near 870 atoms. We ascribe this to the number of atoms, which do not contribute to the magnetic anisotropy. It appears plausible to localize the atoms of vanishing magnetic anisotropy at the rim of the island, within a stripe of width 1–4 atoms [17].

Previously, it has been proposed that edge atoms exhibit a higher magnetic anisotropy, due to their reduced coordination [95]. Our present work shows that coordination effects are comparably less important. Rather, the magnetic properties of Co islands on Cu(1 1 1) appear to be affected by structural and electronic variations near the island edge.

The data for the Fe-decorated island show a very different behavior. The slope of the curve representing a linear fit through the data points indicate a magnetic anisotropy of 0.115 ± 0.005 meV/atom, 22% percent less than for pure Co islands. Remarkably, the fit extrapolates to zero, and there is no indication of a sizable offset. This is in sharp contrast to the result obtained for the pure Co islands.

How can we understand this change of the magnetic anisotropy of the Co island upon decoration? We ascribe this change of the magnetic anisotropy to the decoration-induced lifting of the structural relaxation near the edge of the Co core and to the corresponding change of the electronic structure, as discussed above in section 4. The following outlook addresses the intriguing correlation between structural relaxation and magnetic properties of individual nano structures.

6. Conclusion and outlook

The spin-polarization within single nm small bilayer nano structures has been mapped and quantified by spin-STM. The maps reveal that the spin-polarization at the Fermi energy of a bilayer Co island on Cu(1 1 1) is inverted to negative values in a nm wide rim near the island edge as compared to the island center, where it is positive. The decoration of the Co core by Fe lifts the inverted spin polarization, and the same sign of spin polarization is observed throughout the island. Magnetic field dependent tunneling spectroscopy has been applied to measure the switching fields of individual nano islands in dependence of their size. The quantitive analysis reveals a magnetic anisotropy of 0.148 ± 0.005 meV/atom, where Co atoms at the rim of the island show a vanishing small magnetic anisotropy. Upon Fe-decoration, all Co atoms contribute to the magnetic anisotropy with a reduced value of 0.115 ± 0.005 meV/atom. A spatially resolved study of the electronic structure of individual islands by differential conductance spectroscopy suggests the lifting of structural relaxation in proximity to the island edge upon Fe decoration. In view of the data we speculate that relaxation phenomena of the electronic and geometric structure near the boundary of a nano structure are the key aspects to understand the role of perimetric decoration in this system. From this we infer that the magnetic anisotropy of a nano structure is severely impacted by spatial variations of both spin-dependent electronic properties and structural relaxations.

But what is the link between structural and electronic relaxation and magnetic anisotropy and spin-polarization of

a nano structure? *Ab initio* calculations provide insights into the electronic origin of the strain dependence of the magnetic anisotropy. A strain-driven charge transfer between electronic states of different symmetry near the Fermi energy is a pivotal aspect [96–98].

Clearly, atomic bond lengths and magnetic anisotropy are linked by magneto elastic coupling. However, a word of caution seems to be well justified. Although it is well established for bulk samples and for atomic layers that bond-length variations and magnetic anisotropy are intimately linked via magneto elastic coupling [29, 98–102], the reliable application of the corresponding description for individual nano structures has not been established yet. To appreciate this situation it is necessary to recall that the theoretical modeling of magneto elasticity is very demanding, even for bulk samples and even more so for strained atomic layers [102]. Local variations of bond lengths, such as expected here, may bring this description to its limitations. In view of these structural relaxations and due to the interface nature of all atoms involved in a bilayer nano structure, we conclude that the application of magneto elastic data obtained for bulk and even for strained atomic layers to individual nano structures appears questionable.

Rather, a self-consistent theoretical description of both structural and spin-dependent electronic properties is called for to advance our understanding of the relevant processes on the electronic level. Corresponding calculations for an island with some thousand atoms appear to be beyond present capabilities. Our data may provide a reference for future work in this direction.

Acknowledgments

The authors acknowledge S Ouazi, J Borme, F Donati, S Wedekind, G Rodary, Y Nahas, L Niebergall, P Ignatiev, K Tao, O Brovko and V Stepanyuk for fruitful discussions. We thank N Kurowsky and W Greie for expert technical support. Partial support by DFG SFB 762 is gratefully acknowledged.

References

[1] Weller D and Moser A 1999 Thermal effect limits in ultrahigh-density magnetic recording *Magn. IEEE Trans.* **35** 4423–39
[2] O'Handley R C 2000 *Modern Magnetic Materials: Principles and Applications* (New York: Wiley)
[3] Parkin S, Jiang X, Kaiser C, Panchula A, Roche K and Samant M 2003 Magnetically engineered spintronic sensors and memory *Proc. IEEE* **91** 661–80
[4] Berger A, Supper N, Ikeda Y, Lengsfield B, Moser A and Fullerton E E 2008 Improved media performance in optimally coupled exchange spring layer media *Appl. Phys. Lett.* **93** 122502
[5] Prinz G A 1998 Magnetoelectronics *Science* **282** 1660–3
[6] Wolf S A, Awschalom D D, Buhrman R A, Daughton J M, von Molnr S, Roukes M L, Chtchelkanova A Y and Treger D M 2001 Spintronics: a spin-based electronics vision for the future *Science* **294** 1488–95
[7] Žutić I, Fabian J and Das Sarma S 2004 Spintronics: fundamentals and applications *Rev. Mod. Phys.* **76** 323–410
[8] Bader S D and Parkin S S P 2010 Spintronics *Annu. Rev. Condens. Matter Phys.* **1** 71–88
[9] Eschrig M 2011 Spin-polarized supercurrents for spintronics *Phys. Today* **64** 43–6
[10] Sukhov A and Berakdar J 2008 Temperature-dependent magnetization dynamics of magnetic nanoparticles *J. Phys.: Condens. Matter* **20** 125226
[11] Shaw J M, Russek S E, Thomson T, Donahue M J, Terris B D, Hellwig O, Dobisz E and Chneider M L 2008 Reversal mechanisms in perpendicularly magnetized nanostructures *Phys. Rev.* B **78** 024414
[12] Bauer U, Dabrowski M, Przybylski M and Kirschner J 2011 Experimental confirmation of quantum oscillations of magnetic anisotropy in Co/Cu(0 0 1) *Phys. Rev.* B **84** 144433
[13] Tudosa I, Lubarda M V, Chan K T, Escobar M A, Lomakin V and Fullerton E E 2012 Thermal stability of patterned Co/Pd nanodot arrays *Appl. Phys. Lett.* **100** 102401
[14] Sander D, Oka H, Corbetta M, Stepanyuk V and Kirschner J 2013 New insights into nano-magnetism by spin-polarized scanning tunneling microscopy *J. Electron Spectrosc. Relat. Phenom.* **189** 206–15
[15] Oka H, Ignatiev P A, Wedekind S, Rodary G, Niebergall L, Stepanyuk V S, Sander D and Kirschner J 2010 Spin-dependent quantum interference within a single magnetic nanostructure *Science* **327** 843–6
[16] Oka H, Tao K, Wedekind S, Rodary G, Stepanyuk V S, Sander D and Kirschner J 2011 Spatially modulated tunnel magnetoresistance on the nanoscale *Phys. Rev. Lett.* **107** 187201
[17] Ouazi S, Wedekind S, Rodary G, Oka H, Sander D and Kirschner J 2012 Magnetization reversal of individual co nanoislands *Phys. Rev. Lett.* **108** 107206
[18] Freeman M R and Choi B C 2001 Advances in magnetic microscopy *Science* **294** 1484–8
[19] Oepen H P and Frömter R 2007 *Scanning Electron Microscopy with Polarization Analysis in the Handbook of Magnetism and Advanced Magnetic Materials* **3** (New York: Wiley)
[20] Hankemeier S, Frömter R, Mikuszeit N, Stickler D, Stillrich H, Pütter S, Vedmedenko E Y and Oepen H P 2009 Magnetic ground state of single and coupled permalloy rectangles *Phys. Rev. Lett.* **103** 147204
[21] Lofink F, Hankemeier S, Frömter R, Kirschner J and Oepen H P 2012 Long-time stability of a low-energy electron diffraction spin polarization analyzer for magnetic imaging *Rev. Sci. Instrum.* **83** 023708
[22] Altman M S, Pinkvos H, Hurst J, Poppa H, Marx G and Bauer E 1991 Spin polarized low energy electron microscopy of surface magnetic structure *MRS Proc.* **232** 125–32
[23] Rougemaille N and Schmid A K 2010 Magnetic imaging with spin-polarized low-energy electron microscopy *Eur. Phys. J. Appl. Phys.* **50** 20101
[24] Bader S D 1991 Smoke *J. Magn. Magn. Mater.* **100** 440–54
[25] Ouazi S *et al* 2012 Atomic-scale engineering of magnetic anisotropy of nanostructures through interfaces and interlines *Nature Commun.* **3** 1313
[26] Gambardella P *et al* 2003 Giant magnetic anisotropy of single cobalt atoms and nanoparticles *Science* **300** 1130–3
[27] Stöhr J and Siegmann H C 2006 *Magnetism* (New York: Springer)
[28] Hillion A *et al* 2013 Low temperature ferromagnetism in chemically ordered FeRh nanocrystals *Phys. Rev. Lett.* **110** 087207
[29] Sander D 1999 The correlation between mechanical stress and magnetic anisotropy in ultrathin films *Rep. Prog. Phys.* **62** 809–58
[30] Skomski R 2003 Nanomagnetics *J. Phys.: Condens. Matter* **15** R841–96
[31] Zeppenfeld P, Lutz C P and Eigler D M 1992 Manipulating atoms and molecules with a scanning tunneling microscope *Ultramicroscopy* **4244** 128–33

[32] Crommie M F, Lutz C P and Eigler D M 1993 Confinement of electrons to quantum corrals on a metal surface *Science* **262** 218–20

[33] Fölsch S, Hyldgaard P, Koch R and Ploog K H 2004 Quantum confinement in monatomic Cu chains on Cu(1 1 1) *Phys. Rev. Lett.* **92** 056803

[34] Hirjibehedin C F, Lutz C P and Heinrich A J 2006 Spin coupling in engineered atomic structures *Science* **312** 1021–4

[35] Repp J, Meyer G, Stojković S M, Gourdon A and Joachim C 2005 Molecules on insulating films: scanning-tunneling microscopy imaging of individual molecular orbitals *Phys. Rev. Lett.* **94** 026803

[36] Hamers R J 1989 Atomic-resolution surface spectroscopy with the scanning tunneling microscope *Annu. Rev. Phys. Chem.* **40** 531–59

[37] Kaiser W J and Jaklevic R 1986 Spectroscopy of electrionic states of metals with a scanning tunneling microscooe *IBM J. Res. Dev.* **30** 411–6

[38] Fiete G A and Heller E J 2003 Colloquium: theory of quantum corrals and quantum mirages *Rev. Mod. Phys.* **75** 933–48

[39] Hofer W A, Foster A S and Shluger A L 2003 Theories of scanning probe microscopes at the atomic scale *Rev. Mod. Phys.* **75** 1287–331

[40] Hofer W A 2003 Challenges and errors: interpreting high resolution images in scanning tunneling microscopy *Prog. Surf. Sci.* **71** 147–83

[41] Julliere M 1975 Tunneling between ferromagnetic films *Phys. Lett.* A **54** 225–6

[42] Meservey R and Tedrow P M 1994 Spin-polarized electron tunneling *Phys. Rep.* **238** 173–243

[43] Wulfhekel W and Kirschner J 1999 Spin-polarized scanning tunneling microscopy on ferromagnets *Appl. Phys. Lett.* **75** 1944–6

[44] Bode M 2003 Spin-polarized scanning tunnelling microscopy *Rep. Prog. Phys.* **66** 523

[45] Wiesendanger R 2009 Spin mapping at the nanoscale and atomic scale *Rev. Mod. Phys.* **81** 1495–550

[46] Rodary G, Wedekind S, Oka H, Sander D and Kirschner J 2009 Characterization of tips for spin-polarized scanning tunneling microscopy *Appl. Phys. Lett.* **95** 152513

[47] Corbetta M, Ouazi S, Borme J, Nahas Y, Donati F, Oka H, Wedekind S, Sander D and Kirschner J 2012 Magnetic response and spin polarization of bulk Cr tips for in-field spin-polarized scanning tunneling microscopy *Japan. J. Appl. Phys.* **51** 030208

[48] Phark S, Fischer J A, Corbetta M, Sander D and Kirschner J 2013 Superparamagnetic response of Fe-coated W tips in spin-polarized scanning tunneling microscopy *Appl. Phys. Lett.* **103** 032407

[49] Janis Research Company, LLC (www.janis.com)

[50] Oxford Instruments Omicron NanoScience (www.omicron.de)

[51] Ferrovac GmbH (www.ferrovac.com)

[52] de la Figuera J, Prieto J E, Ocal C and Miranda R 1993 Scanning-tunneling-microscopy study of the growth of cobalt on Cu(1 1 1) *Phys. Rev.* B **47** 13043–6

[53] Diekhöner L, Schneider M A, Baranov A N, Stepanyuk V S, Bruno P and Kern K 2003 Surface states of cobalt nanoislands on Cu(1 1 1) *Phys. Rev. Lett.* **90** 236801

[54] Rastei M V, Heinrich B, Limot L, Ignatiev P A, Stepanyuk V S, Bruno P and Bucher J P 2007 Size-dependent surface states of strained cobalt nanoislands on Cu(1 1 1) *Phys. Rev. Lett.* **99** 246102

[55] Biedermann A, Rupp W, Schmid M and Varga P 2006 Coexistence of fcc- and bcc-like crystal structures in ultrathin fe films grown on Cu(1 1 1) *Phys. Rev.* B **73** 165418

[56] Gerhard L *et al* 2010 Magnetoelectric coupling at metal surfaces *Nature Nanotechnol.* **5** 792–7

[57] Li Bassi A *et al* 2007 Bulk cr tips for scanning tunneling microscopy and spin-polarized scanning tunneling microscopy *Appl. Phys. Lett.* **91** 173120

[58] Schlenhoff A, Krause S, Herzog G and Wiesendanger R 2010 Bulk Cr tips with full spatial magnetic sensitivity for spin-polarized scanning tunneling microscopy *Appl. Phys. Lett.* **97** 083104

[59] Nagai S, Hata K, Oka H, Sander D and Kirschner J 2014 Atomic structure and spin polarization at the apex of tips used in spin-polarized scanning tunneling microscopy *Appl. Phys. Express* **7** 025204

[60] Nagai S, Sakakibara H, Hata K, Okada M and Mimura H 2011 Measurement of *z*-direction component of electron spins field-emitted from a single-crystal magnetite whisker *Ultramicroscopy* **111** 405–8

[61] Pietzsch O, Kubetzka A, Bode M and Wiesendanger R 2004 Spin-polarized scanning tunneling spectroscopy of nanoscale cobalt islands on Cu(1 1 1) *Phys. Rev. Lett.* **92** 057202

[62] Slonczewski J C 1989 Conductance and exchange coupling of two ferromagnets separated by a tunneling barrier *Phys. Rev.* B **39** 6995–7002

[63] Wortmann D, Heinze S, Kurz Ph, Bihlmayer G and Blügel S 2001 Resolving complex atomic-scale spin structures by spin-polarized scanning tunneling microscopy *Phys. Rev. Lett.* **86** 4132–5

[64] Yuasa S, Nagahama T and Suzuki Y 2002 Spin-polarized resonant tunneling in magnetic tunnel junctions *Science* **297** 234–7

[65] Oka H, Rodary G, Wedekind S, Ignatiev P A, Niebergall L, Stepanyuk V S, Sander D and Kirschner J 2011 New insights into nanomagnetism: spin-polarized scanning tunneling microscopy and spectroscopy studies *Spintronics* IV **8100** 81000O

[66] Rodary G, Wedekind S, Sander D and Kirschner J 2008 Magnetic hysteresis loop of single Co nano-islands *Japan. J. Appl. Phys.* **47** 1913–5

[67] Yamada T K, Bischoff M M J, Heijnen G M M, Mizoguchi T and van Kempen H 2003 Observation of spin-polarized surface states on ultrathin bct mn(0 0 1) films by spin-polarized scanning tunneling spectroscopy *Phys. Rev. Lett.* **90** 056803

[68] Donati F, Fratesi G, Ning L, Brambilla A, Trioni M I, Li Bassi A, Casari C S and Passoni M 2013 Electronic and magnetic properties of bulk cr tips for scanning tunneling spectroscopy *Phys. Rev.* B **87** 235431

[69] Heller E J, Crommie M F, Lutz C P and Eigler D M 1994 Scattering and absorption of surface electron waves in quantum corrals *Nature* **369** 464–6

[70] Hasegawa Y and Avouris P 1993 Direct observation of standing wave formation at surface steps using scanning tunneling spectroscopy *Phys. Rev. Lett.* **71** 1071–4

[71] Pietzsch O, Okatov S, Kubetzka A, Bode M, Heinze S, Lichtenstein A and Wiesendanger R 2006 Spin-resolved electronic structure of nanoscale cobalt islands on Cu(1 1 1) *Phys. Rev. Lett.* **96** 237203

[72] Oka H, Brovko O, Corbetta M, Stepnayuk V, Sander D and Kirschner J 2014 Spin-polarized quantum confinement in nanostructures *Rev. Mod. Phys.* at press

[73] Niebergall L, Stepanyuk V S, Berakdar J and Bruno P 2006 Controlling the spin polarization of nanostructures on magnetic substrates *Phys. Rev. Lett.* **96** 127204

[74] Wedekind S 2010 A spin-polarized scanning tunneling microscopy and spectroscopy study of individual nanoscale particles grown obn copper surfaces *PhD Thesis* University Halle-Wittenberg

[75] Corbetta M 2013 Spin-polarized scanning tunneling microscopy and spectroscopy study of Fe and Co nanostructures on Cu(1 1 1) *PhD Thesis* University Halle-Wittenberg

[76] Phark S h, Corbetta M, Fischer J A, Oka H, Ouazi S, Sander D and Kirschner J 2014 *Nature Commun.* submitted
[77] Brune H 1998 Microscopic view of epitaxial metal growth: nucleation and aggregation *Surf. Sci. Rep.* **31** 125–229
[78] Hanbücken M and Deville J P 2001 *Stress and Strain in Epitaxy: Theoretical Concepts, Measurements and Applications* (Amsterdam: Elsevier)
[79] Kern R and Müller P 1997 Elastic relaxation of coherent epitaxial deposits *Surf. Sci.* **392** 103–33
[80] Stepanyuk V S, Tsivlin D V, Sander D, Hergert W and Kirschner J 2003 Mesoscopic scenario of strain-relief at metal interfaces *Thin Solid Films* **428** 1–5
[81] Müller B, Fischer B, Nedelmann L, Fricke A and Kern K 1996 Strain relief at metal interfaces with square symmetry *Phys. Rev. Lett.* **76** 2358–61
[82] Mironets O, Meyerheim H L, Tusche C, Stepanyuk V S, Soyka E, Zschack P, Hong H, Jeutter N, Felici R and Kirschner J 2008 Direct evidence for mesoscopic relaxations in cobalt nanoislands on Cu(0 0 1) *Phys. Rev. Lett.* **100** 096103
[83] Meyerheim H L, Crozier E D, Gordon R A, Xiao Q F, Mohseni K, Negulyaev N N, Stepanyuk V S and Kirschner J 2012 Direct proof of mesoscopic misfit in nanoscale islands by x-ray absorption spectroscopy *Phys. Rev.* B **85** 125405
[84] Rastei M V, Bucher J P, Ignatiev P A, Stepanyuk V S and Bruno P 2007 Surface electronic states in Co nanoclusters on Au(1 1 1): scanning tunneling spectroscopy measurements and *ab initio* calculations *Phys. Rev.* B **75** 045436
[85] Donati F, Fratesi G, Passoni M, Casari C S, Mairov A, Bottani C E, Trioni M I and Li Bassi A 2011 Strain effect on local electronic properties of Fe nanoislands grown on Au(1 1 1) *Phys. Rev.* B **83** 153404
[86] Lysenko O V, Stepanyuk V S, Hergert W and Kirschner J 2002 Mesoscopic relaxation in homoepitaxial growth *Phys. Rev. Lett.* **89** 126102
[87] Cerda J R, de Andres P L, Cebollada A, Miranda R, Navas E, Schuster P, Schneider C M and Kirschner J 1993 Epitaxial growth of cobalt films on Cu(1 0 0): a crystallographic leed determination *J. Phys.: Condens. Matter* **5** 2055
[88] Ibach H 1997 The role of surface stress in reconstruction, epitaxial growth and stabilization of mesoscopic structures *Surf. Sci. Rep.* **29** 195–263
[89] Sander D 2003 Surface stress: implications and measurements *Curr. Opin. Solid State Mater. Sci.* **7** 51–7
[90] Kneller E F and Luborsky F E 1963 Particle size dependence of coercivity and remanence of single-domain particles *J. Appl. Phys.* **34** 656–8
[91] Brown W F 1963 Thermal fluctuations of a single-domain particle *Phys. Rev.* **130** 1677–86
[92] Brown W F 1959 Relaxational behavior of fine magnetic particles *J. Appl. Phys.* **30** S130–2
[93] Bean C P and Livingston J D 1959 Superparamagnetism *J. Appl. Phys.* **30** S120–9
[94] Stoner E C and Wohlfarth E P 1948 A mechanism of magnetic hysteresis in heterogeneous alloys *Phil. Trans. R. Soc. Lond. Ser. A: Math. Phys. Sci.* **240** 599–642
[95] Rusponi S, Cren T, Weiss N, Epple M, Buluschek P, Claude L and Brune H 2003 The remarkabe difference between surface and step atoms in the magnetic anisotropy of two-dimensional nanostructures *Nature Mater.* **2** 546–51
[96] Wu R, Chen L J, Shick A and Freeman A J 1998 First-principles determinations of magneto-crystalline anisotropy and magnetostriction in bulk andthin-film transition metals *J. Magn. Magn. Mater.* **177–81** 1216–9
[97] Wu R 2001 First rinciples determination of magnetic anisotropy and magnetostriction in transition metal alloys chapter part I, *Lecture Notes in Physics: Band-Ferromagnetism* (Berlin: Springer) pp 46–71
[98] Sander D 2004 The magnetic anisotropy and spin reorientation of nanostructures and nanoscale films *J. Phys.: Condens. Matter* **16** R603–36
[99] Kittel C 1949 Physical theory of ferromagnetic domains *Rev. Mod. Phys.* **21** 541–83
[100] Gutjahr-Löser T, Sander D and Kirschner J 2000 Magnetoelastic coupling in Ni and Fe monolayers on Cu(0 0 1) *J. Appl. Phys.* **87** 5920–2
[101] Sander D, Pan W, Ouazi S, Kirschner J, Meyer W, Krause M, Müller S, Hammer L and Heinz K 2004 Reversible h-induced switching of the magnetic easy axis in Ni/Cu(0 0 1) thin films *Phys. Rev. Lett.* **93** 247203
[102] Sander D and Kirschner J 2011 Non-linear magnetoelastic coupling in monolayers: experimental challenges and theoretical insights *Phys. Status Solidi* b **248** 2389–97